(This is a sample cover image for this issue. The actual cover is not yet available at this time.)

Earth and Planetary Science Letters 317-318 (2012) 185–195

Contents lists available at SciVerse ScienceDirect

Earth and Planetary Science Letters

journal homepage: www.elsevier.com/locate/epsl

Evidence for northeastern Tibetan Plateau uplift between 25 and 20 Ma in the sedimentary archive of the Xining Basin, Northwestern China

Guoqiao Xiao [a,b], Zhengtang Guo [c,*], Guillaume Dupont-Nivet [d,e,f], Houyuan Lu [c], Naiqin Wu [c], Junyi Ge [c], Qingzhen Hao [c], Shuzhen Peng [g], Fengjiang Li [c], Hemmo A. Abels [h], Kexin Zhang [b]

[a] State Key Laboratory of Loess and Quaternary Geology, Institute of Earth Environment, Chinese Academy of Sciences, P.O. Box 17, Xian, 710075, China
[b] State Key Laboratory of Biogeology and Environmental Geology, China University of Geosciences, Wuhan, 430074, China
[c] Key Laboratory of Cenozoic Geology and Environment, Institute of Geology and Geophysics, Chinese Academy of Sciences, Beijing, 100029, China
[d] Geosciences Rennes UMR 6118-CRNS, Université de Rennes 1, Campus de Beaulieu, 35042 Rennes Cedex, France
[e] Paleomagnetic Laboratory 'Fort Hoofddijk', Dept. of Earth Sciences, Utrecht University, Utrecht, The Netherlands
[f] Key Laboratory of Orogenic Belts and Crustal Evolution, Ministry of Education (Peking Unviersity), Beijing 100871, PR China
[g] Taishan College, Tai'an 271021, China
[h] Stratigraphy/Paleontology, Dept. of Earth Sciences, Utrecht University, Utrecht, The Netherlands

ARTICLE INFO

Article history:
Received 4 June 2011
Received in revised form 11 November 2011
Accepted 12 November 2011
Available online xxxx

Editor: T.M. Harrison

Keywords:
NE Tibet
magnetostratigraphy
tectonic uplift
paleoclimate
sedimentary provenance
Xining Basin

ABSTRACT

The growth history of the Tibetan Plateau provides a valuable natural laboratory to understand tectonic processes of the India–Asia collision and their impact on and interactions with Asian and global climate change. However, both Tibetan Plateau growth and Asian paleoenvironments are generally poorly documented in pre-Pliocene times and reflect limited temporal coverage for different parts of the plateau. Here we present magnetostratigraphic results from the Xining Basin, at the NE margin of the Tibetan Plateau, precisely dating the record between the earliest Oligocene (~33 Ma) to the middle Miocene (~16 Ma). The pattern of observed paleomagnetic polarity zones is unequivocally correlated to the geomagnetic polarity time scale (GPTS) indicating relatively constant and low sediment accumulation rates (32 m/Myr) except for a peculiar period of unstable accumulation between 25.3 and 19.7 Ma. At the beginning of this interval, a marked permanent increase in magnetite content of the sediments is observed and likely relates to a change in provenance. We directly relate this unstable period of sediment accumulation and provenance change to the coeval exhumation recently reported by low-temperature thermochronology from the Laji Shan range, which subsequently formed the southern margin of the Xining Basin. Evidence for NE Tibet tectonism at 25–20 Ma can be associated with widespread deformation over the entire Himalayan–Tibetan orogen at this time, which may be linked to the coeval appearance of monsoon climate in Eastern Asia and the onset of central Asian desertification.

1. Introduction

The timing of the growth of the Himalayan–Tibetan Plateau has profound implications for understanding the mechanics of continental deformation (e.g., Dayem et al., 2009; Harrison et al., 1992; Royden et al., 2008; Tapponnier et al., 2001) and associated regional and global climatic changes in the Cenozoic (e.g., Kent and Muttoni, 2008; Molnar et al., 2010; Raymo and Ruddiman, 1992). Various lines of evidence provided by previous tectonic studies from different parts of the plateau have suggested a wide range of uplift models and thus different histories of plateau growth (e.g., Harrison et al., 1992; Molnar and Stock, 2009; Molnar et al., 1993; Tapponnier et al., 2001; Wang et al., 2008). Climate studies have suggested that the appearance of the monsoonal system in East Asia and the onset of central Asian desertification may be related to Cenozoic Himalayan–Tibetan uplift and withdrawal of the Paratethys Sea (Clift et al., 2008; Guo et al., 2002, 2008; Ramstein et al., 1997; Sun and Wang, 2005; Zhang et al., 2007a, 2007b). In addition, surface uplift of various parts of the Tibetan Plateau may have affected differently either the East Asian monsoon or the Indian monsoon which, from an atmospheric dynamics perspective, are different climate phenomena and are probably forced by different boundary conditions (e.g., Boos and Kuang, 2010; Molnar et al., 2010). To further constrain the surface uplift history of the Himalayan–Tibetan Plateau and its relationship with the Asian climate change, more precise age constraints on the plateau growth and paleoenvironmental evolution from different parts of the plateau are still required.

Here we report a well-dated sedimentary record from the Xining Basin at the northeastern margin of the Tibetan Plateau. The study area has recently received increasing attention because it is ideally located to investigate when and how the plateau grew northward and is within the transitional belt of the East Asian monsoonal humid areas and the northwest arid areas such that it is sensitive to

* Corresponding author.
E-mail address: ztguo@mail.iggcas.ac.cn (Z. Guo).

0012-821X/$ – see front matter © 2011 Elsevier B.V. All rights reserved.
doi:10.1016/j.epsl.2011.11.008

changes in the monsoonal climate (e.g., Dai et al., 2006; Dettman et al., 2003; Dupont-Nivet et al., 2003, 2004, 2008a, 2008b; Fang et al., 2003, 2005; Garzione et al., 2005; Horton et al., 2004; Hough et al., 2011; Ji et al., 2010; Lease et al., 2007, 2011, in press; Li et al., 1997; Lu et al., 2004; Pares et al., 2003; Wang and Deng, 2005; Yue et al., 2001; Zheng et al., 2003, 2006). The tectonic history of this region, however, still remains controversial. According to the northward stepwise growth model (Tapponnier et al., 2001), the NE Tibetan Plateau mainly grew during Pliocene to Quaternary times. However, other studies have yielded evidence for tectonism and surface uplift ranging from late Eocene to early Pleistocene, including magnetostratigraphic dating of sediment accumulation rates and/or occurrence of thick conglomerate deposits (Dai et al., 2006; Fang et al., 2003, 2005; Horton et al., 2004; Ji et al., 2010; Li et al., 1997; Pares et al., 2003), ages of fluvial terraces (Lu et al., 2004), thermochronological studies (Clark et al., 2010; Lease et al., 2011; Zheng et al., 2003, 2006), tectonic rotation studies (Dupont-Nivet et al., 2004, 2008a; Yan et al., 2006), detrital zircon U–Pb ages (Lease et al., 2007, in press), Nd isotopic studies (Garzione et al., 2005), carbon and oxygen isotope-based paleoaltimetry and/or topographic evolution (Dettman et al., 2003; Hough et al., 2011; Wang and Deng, 2005), and occurrence of high-altitude pollen assemblages (Dupont-Nivet et al., 2008b).

With a thick sequence of Paleocene to early Miocene lacustrine records, the Xining Basin at the NE margin of the Tibetan Plateau (Fig. 1a) provides an important sedimentary archive for understanding the paleoclimate and surface uplift history of this region (QBGMR, 1985, 1991). It is only in recent years that the magnetostratigraphy and the paleoenvironmental change of this basin have been studied (Abels et al., 2011; Dai et al., 2006; Dupont-Nivet et al., 2007; Horton et al., 2004; Wu et al., 2006; Xiao et al., 2010). However, these studies have mainly focused on the late Eocene to early Oligocene, with little attention to the paleoenvironmental changes recorded in the Miocene strata that may be associated with the growth of the Tibetan Plateau. Furthermore, while the Paleogene strata provided reliable magnetostratigraphic correlations, the results for the Miocene deposits in the Xining Basin have proven to be controversial (Dai et al., 2006; Wu et al., 2006). Remarkably, the onset of accelerated exhumation of the Laji Shan range, which makes up the southern edge of the Xining Basin, revealed to be earliest Miocene (ca. 22 Ma) by a recent thermochronological study (Lease et al., 2011), has not been detected in the sedimentary record of the Xining Basin. In this study, we present a detailed magnetostratigraphy and magnetic susceptibility investigation of the Xining Basin sedimentary record with a view to achieving a better understanding of the Oligocene to Miocene tectonism and paleoenvironments of the NE Tibetan Plateau.

2. Geological setting

The Xining Basin lies at the northeastern edge of the Tibetan Plateau, with elevations mainly between ~2300 and ~3000 m (Fig. 1a). Climatically, the Xining Basin lies in the transitional belt of the East Asian monsoonal humid areas and the northwest arid areas, dominated by an arid/semiarid continental climate. At present, the mean annual temperature and precipitation in this area are 6.06 °C and 415 mm, respectively, with over 70% of the precipitation falling from June to September.

The Xining Basin has been interpreted as a Late Jurassic–Early Cretaceous fault-related basin, characterized by slow subsidence rates until the Neogene, when faults were reactivating and compartmentalizing the basin (Horton et al., 2004). The basin is bounded by the Laji Shan Fault to the south and the middle Qilian Shan Fault to the north (Fig. 1b). With a thickness of more than 800 m, the well-developed Cenozoic stratigraphy in the Xining Basin has been divided into six formations: Qijiachuan, Honggou, Mahalagou, Xiejia, Chetougou, and Xianshuihe Formations in upward sequence (QBGMR, 1985, 1991). Recent paleomagnetic investigations from the Xiejia and Shuiwan sections indicate that the Cenozoic stratigraphy of the Xining Basin spans from ~55 Ma to 17 Ma (Dai et al., 2006), consistent with the biostratigraphic age (Hao et al., 1983; Horton et al., 2004; Li and Qiu, 1980; Li et al., 1981; QBGMR, 1985, 1991; Qiu and Qiu, 1995; Wang et al., 1990). The stratigraphy consists of basal sandy and gypsiferous successions (Qijiachuan Formation) overlain by red mudstones with distinctive gypsiferous cyclic intercalations (Honggou and Mahalagou Formations) overlain by light brown to yellow mudstones with occasional sandy lenses (Xiejia, Chetougou and Xianshuihe Formations) (QBGMR, 1985, 1991).

Our study focuses on the Xiejia, Chetougou and Xianshuihe Formations. The studied Tashan (TS) section is situated in the mid-southern part of the Xining Basin, ~7 km south of the Xining city, and ~25 km north of the present-day position of the Laji Shan range

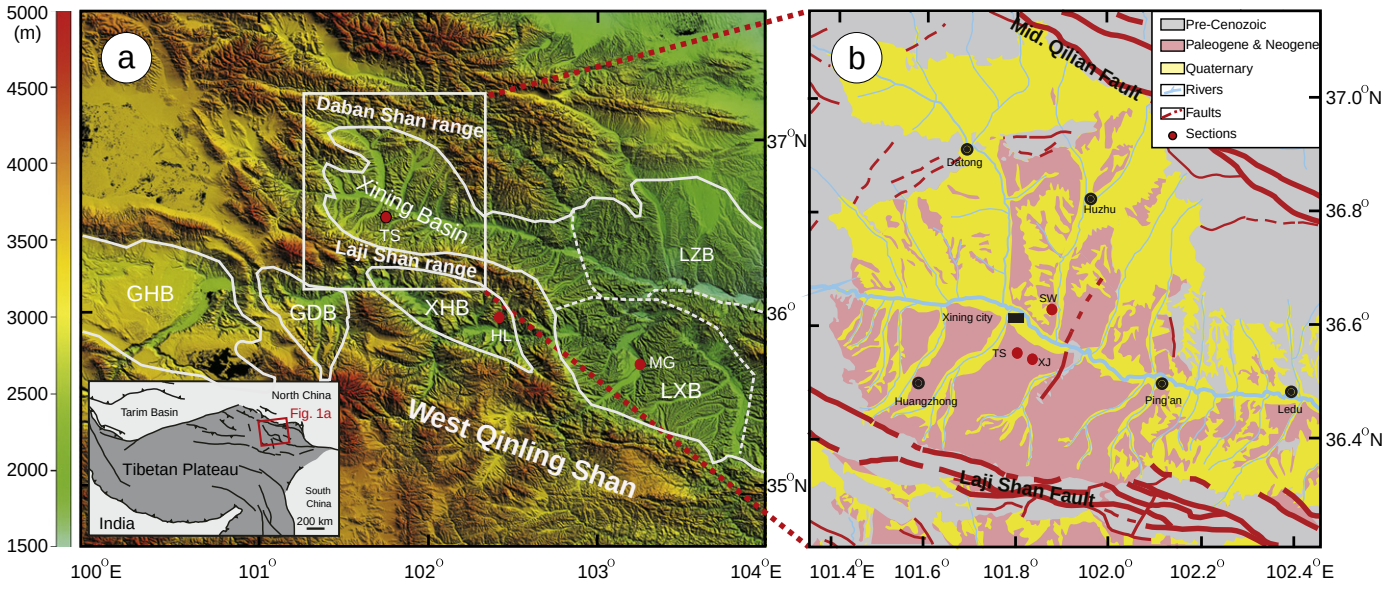

Fig. 1. (a) Topographic map of the NE Tibetan Plateau showing the location of the Xining Basin, and other basins and sections discussed in the text are also labeled. GDB, Guide Basin; GHB, Gonghe Basin; XHB, Xunhua Basin; LZB, Lanzhou Basin; LXB, Linxia Basin; HL, Hualong section (Lease et al., in press); MG, Maogou section (Fang et al., 2003). (b) Geological map shows the location of the Tashan (TS), the Xiejia (XJ), and the Shuiwan (SW) sections.

(Fig. 1). The composite TS section measures 560.9 m in thickness and consists of seven subsections near the Tashan village (101°50′E, 36°33′N). We report here the upper six subsections (total 457.5 m in thickness) of the TS section that complement results from the bottom subsection (103.4-m thick) reported by Xiao et al. (2010). An additional ~60 m of the Xianshuihe Formation above our section has not been sampled because this interval is poorly exposed. In the field, the subsections have been correlated by marker layers that can be traced more than 5 km. Also, using these marker layers, the TS section can be straightforwardly correlated to the Xiejia section that is located ~3 km to the east (Fig. 1b). According to previous descriptions of the Xiejia section (Li and Qiu, 1980; QBGMR, 1985), the well-known Xiejia Fauna (Qiu and Qiu, 1995) was found in bed 39 of the described Xiejia section (QBGMR, 1985); it is ~10 m above a notable green gypsiferous layer referred to as the "green belt" (bed 37 of the described Xiejia section; QBGMR, 1985), which has been defined as the boundary between the Mahalagou and the Xiejia Formations (QBGMR, 1985). This "green belt" and the layer of the Xiejia Fauna can be traced laterally in all outcrops. In the TS section, they correspond to the depth of ~261 m and ~252 m, respectively (Fig. 2a). In this study, we follow the definition for the Mahalagou, Xiejia, and Chetougou Formations of the 1:50,000 geological mapping (QBGMR, 1985) and not of Dai et al. (2006) who used a different definition. Based on the depth of the marker layers and the thickness of each formation as described in the Xiejia section (Liu, 1992; QBGMR, 1985), we recognized the Mahalagou (below 260 m), Xiejia (160–260 m), Chetougou (90–160 m), and Xianshuihe (above 90 m) Formations. We noted an abrupt sediment color change (Fig. 2b), found at the depth of ~160 m, which is consistent with the boundary between the Xiejia and the Chetougou Formations (QBGMR, 1985).

3. Sampling and methods

In this study, a total of 1811 oriented block samples were collected with sample spacing of 25 cm for paleomagnetic investigation. 2 cm cubic specimens were cut from each oriented block sample. All specimens were subjected to progressive thermal demagnetization in a MMTD-80 thermal demagnetizer. Thermal demagnetization up to 690 °C included a maximum of 16 steps with intervals of 50 °C below 585 °C and 20–30 °C above. Remanence measurements were made using a 2G-760 cryogenic magnetometer and performed in the Paleomagnetism and Geochronology Laboratory of the Institute of Geology and Geophysics, Chinese Academy of Sciences, Beijing, China, where all equipment is installed in a magnetically shielded room (background field<300 nT).

In order to explore the magnetic mineralogy of the TS section, six samples from different depths within the composite section were selected for thermomagnetic analysis (magnetic susceptibility versus temperature curves), using an AGICO CS-3 apparatus coupled to a KLY-3 kappabridge. In addition, 4549 samples at 10-cm stratigraphic intervals were collected for magnetic susceptibility analyses, using a Bartington MS2 meter.

4. Results

4.1. Characteristic Remanent Magnetization (ChRM) analysis

Demagnetization results were evaluated on stereographic projections and vector end point orthogonal diagrams (Fig. 3a–i). For most samples, after removing a viscous magnetization component below 250–350 °C, a Characteristic Remanent Magnetization (ChRM) component was successfully isolated between 350 °C and 650 °C (up to 670 °C) with most of the remanence demagnetized at ~585 °C. This suggests a combination of magnetite and hematite, further supported by the thermomagnetic analysis results presented below (Fig. 4). A small number of samples (6.8%), mostly from gypsiferous beds and/or green mudstone beds, showed very low natural remanent magnetization (NRM) intensity and unstable demagnetization trajectories such that ChRM directions could not be isolated. For the remaining samples, the ChRM directions were calculated on a minimum of four consecutive steps (Kirschvink, 1980). ChRM directions with maximum angular deviation (MAD) above 15° were rejected from further analyses. To remove outliers and transitional directions, we further rejected normal and reverse ChRM directions with Virtual Geomagnetic Poles (VGP) more than 45° from the mean normal and reverse VGP respectively. The remaining 1502 ChRM reliable directions (82.9%) cluster in antipodal fashion, although the reversals test (Tauxe, 1998) is negative (at 95% confidence) due to a slight bias of the mean normal directions ($D=5.2°$; $I=40.2°$; $\alpha_{95}=1.5°$; $k=14.7$; $n=649$) towards the North and of the mean reversed direction ($D=191.6°$; $I=-40.0°$; $\alpha_{95}=1.2°$; $k=16.6$; $n=853$) towards the West. This small bias may result from small vertical-axis rotation throughout the time span of the section or, as explained in Dupont-Nivet et al. (2008a, b; see their Fig. 7), it may relate to the incomplete separation of the normal overprint in some of the ChRM directions. In any case, this does not alter the reliability of the polarity determination on these directions.

The above ChRM directions of 1502 samples are used to calculate the virtual geomagnetic pole latitudes and define the geomagnetic polarity zones. Polarity zones are defined by at least two successive levels of similar polarity. Together with the previous work of Xiao et al. (2010; gray dots and polarity in Fig. 5) for the bottom 103.3 m of the TS section, a total of 23 pairs of normal (N1 to N23, Fig. 5) and reversed (R1 to R23) polarity zones are identified in the composite TS section.

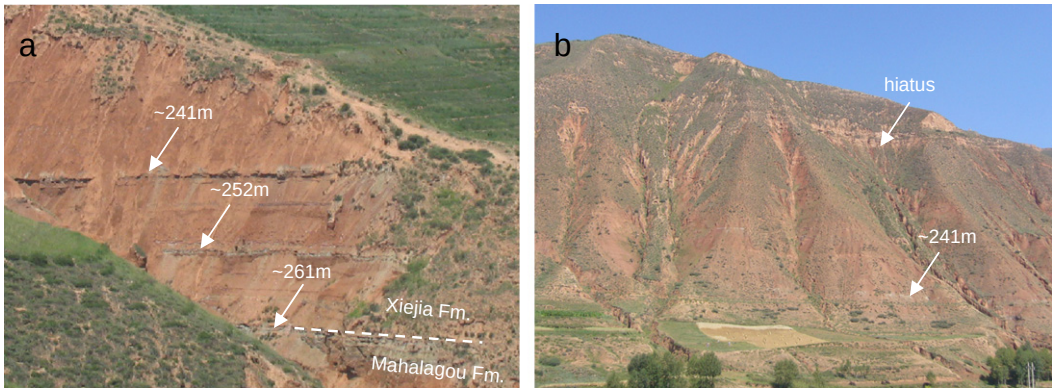

Fig. 2. (a) The boundary of Mahalagou and Xiejia Formations and other marker layers of the Tashan section. (b) View of the hiatus found at the depth of ~160 m of the Tashan section.

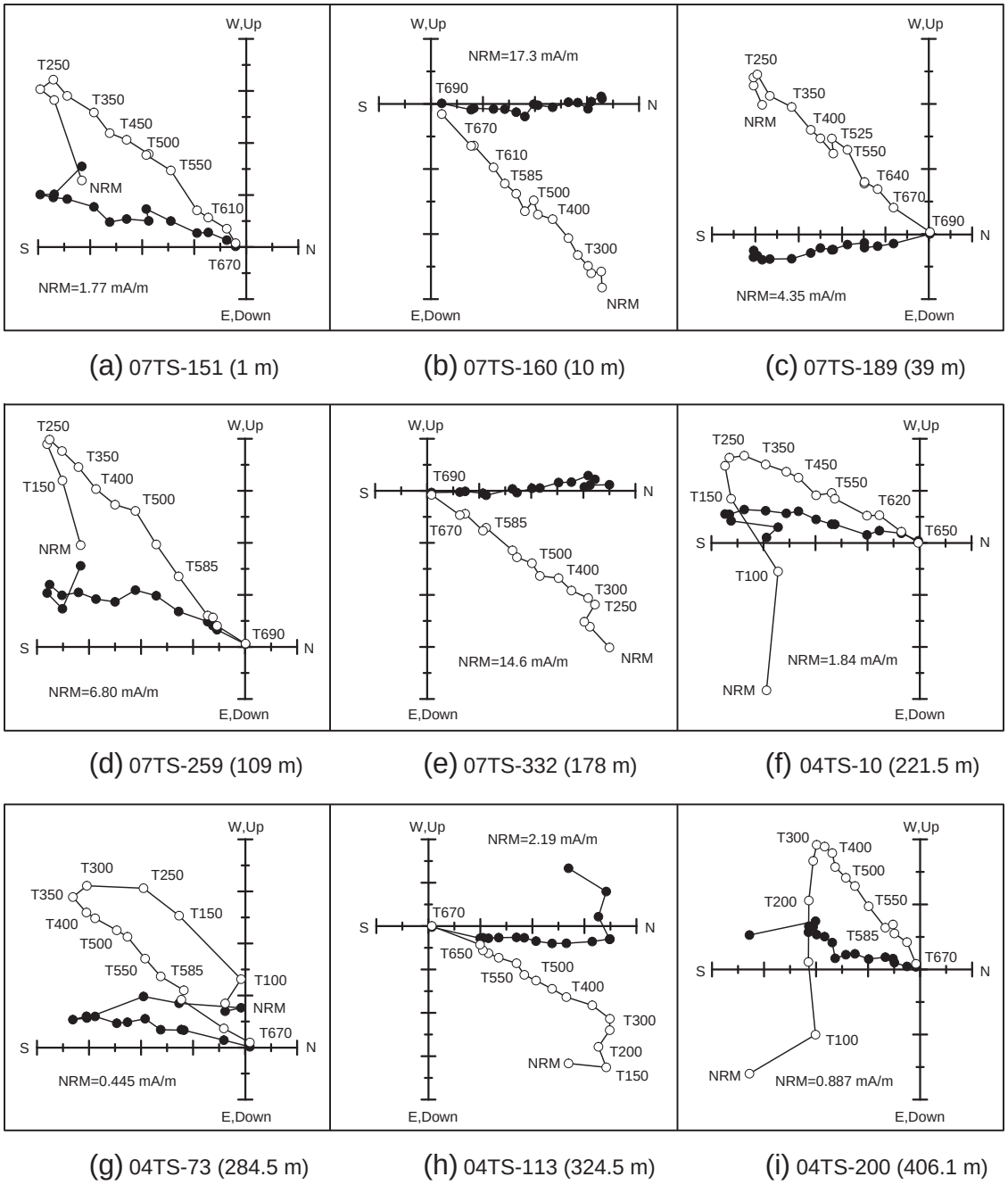

Fig. 3. Orthogonal (Zijderveld) vector plots of representative thermal demagnetization behaviors of specimens from the TS section (a–i). The solid and open circles represent vector end-points projected onto horizontal and vertical planes, respectively. NRM is the natural remanent magnetization before demagnetization.

4.2. Rock magnetic analysis

The results from the demagnetization described above (Fig. 3) and from thermomagnetic analysis (Fig. 4) show that all the samples exhibit a noticeable decrease in magnetic susceptibility near the Curie temperatures of both magnetite and hematite. The signature of hematite in these samples suggests the magnetic minerals in the TS section consist of a combination of hematite and magnetite, similar to the nearby Xiejia and Shuiwan sections (Dai et al., 2006; Dupont-Nivet et al., 2007).

Stratigraphically, the magnetic susceptibility of the TS section exhibits an abrupt and significant upward increase at the depth of ~250 m (Fig. 6). This increase is most likely related to an increase in the magnetite content of the mineral composition of the sediment for the following reasons. The susceptibility of magnetite is over three orders of magnitude higher than that of hematite and much higher than other minerals most commonly found in red beds (Dunlop and Özdemir, 1997) and therefore will dominate any susceptibility change. The change of the magnetic mineral composition of the sediments can also be reflected by the ratios of remanence intensity after thermal demagnetization. The remanence intensity ratios of $J_{150\ °C}/J_{NRM}$, $J_{400\ °C}/J_{150\ °C}$, and $J_{610\ °C}/J_{NRM}$ have been interpreted as qualitative indicators of the remanence contributed by goethite, maghemite, and hematite, respectively (Gautam and Fujiwara, 2000). Our thermal demagnetization results (Fig. 3) show that, for most samples, the temperature required for the removal of the viscous magnetization component is between 250 °C and 350 °C, so here we use the ratio of $(J_{400\ °C}-J_{585\ °C})/J_{400\ °C}$ to qualitatively evaluate

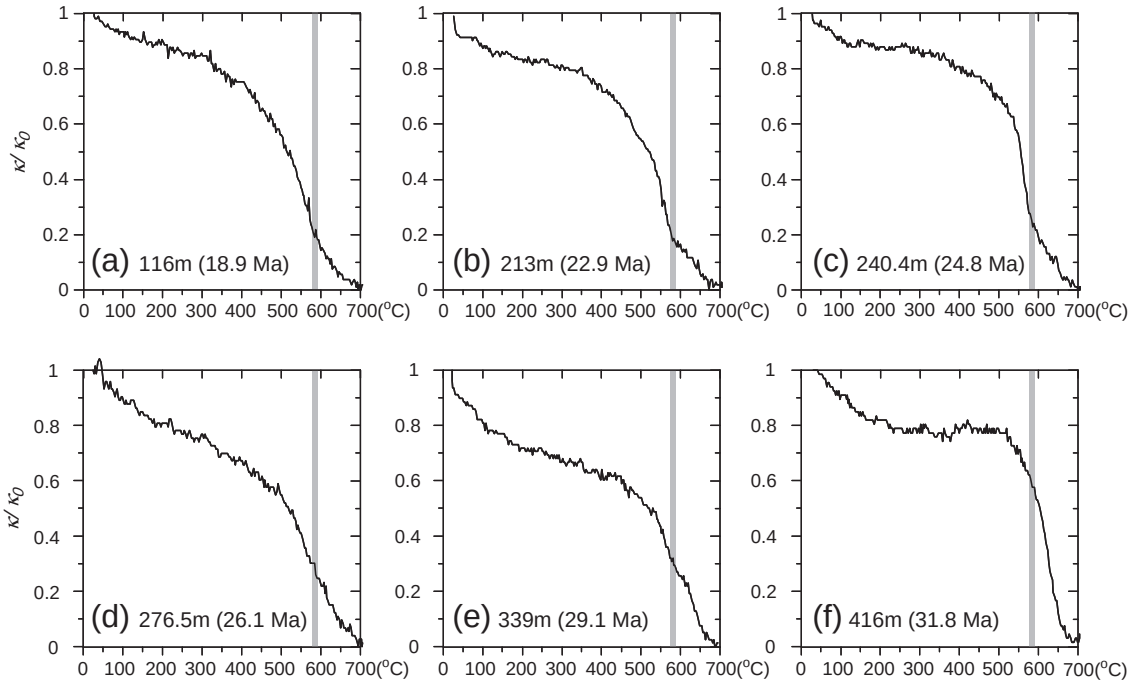

Fig. 4. Temperature dependence of magnetic susceptibility from different depth of the TS section (see Fig. 6 for sample positions). The gray bar in each plot indicates the Curie temperature of magnetite. Note that the samples above ~250 m (~25 Ma) have relatively higher magnetite concentrations than samples below.

the content of magnetite. As shown in Fig. 6, a noticeable increase in the ratios of $(J_{400\ °C}–J_{585\ °C})/J_{400\ °C}$ occurs at the depth of ~250 m as expected for an increase in magnetite content. Finally, thermomagnetic analysis above ~250 m exhibits a noticeable decrease in magnetic susceptibility at ~580 °C (Fig. 4a, b, c), while the samples below do not show such a decrease (Fig. 4d, e, f), again supporting that sediments from the upper part of the TS section have relatively higher magnetite concentrations than the lower part.

5. Age constraints on the Xining Basin sediments

5.1. Correlation to the geomagnetic polarity time scale (GPTS)

The obtained magnetozones can be divided into four intervals according to their characteristics: the intervals R1-N8 (0–195.9 m) and R14-N19 (246.9–395.7 m) are characterized by interbedded moderate long normal and reversed polarity zones, e.g., N1, R3, N5, N6, R7, N7, N8, R14, N14, N15, and N17 (Fig. 5); the interval R9-N13 (195.9–246.9 m) is characterized by frequent occurrence of short polarity zones, e.g., N9, N10, N11, N12, and N13; and the interval R20-N23 (395.7–560.9) contains two remarkably long reversed polarity zones (R20 and R22, ~70 m and ~65 m in length, respectively). Based on the biostratigraphic age of early Miocene for the Xiejia Fauna (Qiu and Qiu, 1995), the most plausible correlation of these remarkably long R20 and R22 intervals is to the particularly long chrons C12r and C13r (Fig. 5) of the GPTS of Gradstein et al. (2004) (hereinafter referred to as GTS04), respectively. Accordingly, the magnetozones of N14–N19 can be readily matched with the C8n–C12n. This correlation is in line with the previous studies that the N20–N23 is correlated with C13n–C16n.1n of GTS04 (Abels et al., 2011; Dupont-Nivet et al., 2007; Xiao et al., 2010). The upper part of the TS section (R1–R7, 0–160 m) correlates well with the chrons C5Br–C6r, with the two successive long normal polarity intervals (N5 and N6) correlated with C5En and C6n, respectively. This correlation is in line with the biostratigraphic age for Chetougou Formation as middle Miocene (Wang et al., 1990).

The upper part (R1–R7, 0–160 m) and lower part (N14–N23, 260–560 m) could be readily matched to the GTS04 time scale, but the remaining magnetozones N7–R14 (160–263.6 m) in the middle part of the section do not show the pattern of chrons C6A–C7A expected between ~20 and 25.3 Ma (gray area in Fig. 5). Our high-resolution sampling ensures we have correctly documented the polarity pattern in the TS section. Also, the rock magnetic properties throughout this peculiar interval do not show particular characteristics that could explain the discrepancy.

The color change associated with the transition from the Xiejia to Chetougou Formation found at ~160 m (Fig. 2a) could mark a hiatus from 21.7 to 20.0 Ma allowing correlation of long normal zones N7 and N8 approximately to chrons C6Bn.1n and 2n. Upwards from N14 to this hiatus, the correlation remains enigmatic and two options are given (Fig. 5). Correlation I relates the three short intervals (N9, N10, and N11) with C6Cn.1n, C6Cn.2n, and C6Cn.3n, respectively (Fig. 5), while correlation II relates the long reversed polarity R13 and short N13 to C6Cr and C7n.1n, respectively. However, the magnetozones between N9 and N12 do show a pattern different from that of C6Cn, indicating variable sediment accumulation rates (Fig. 7a, b). In any case, the interval from 25.3 to 20.0 Ma does not show a good fit with the polarity time scale, while above and below very straightforward correlations can be made. The lack of a satisfactory correlation in this peculiar interval thus indicates that the recording of the magnetozones in the sedimentary record was not continuous, as a result of hiatuses (gaps in sediment accumulation), variable sediment accumulation rates, or both. In summary, unstable sedimentation rates occur from 25.3 to 19.7 Ma, of which the base coincides with the change to increased magnetite content of the sediments, and the top to a hiatus between 21.7 and 20.0 Ma. The tectonic and paleoenvironmental interpretations of these results are discussed below.

5.2. Xining Basin stratigraphy

Previous attempts to date the Xining Basin record using magnetostratigraphy are reported by Dai et al. (2006) and Wu et al.

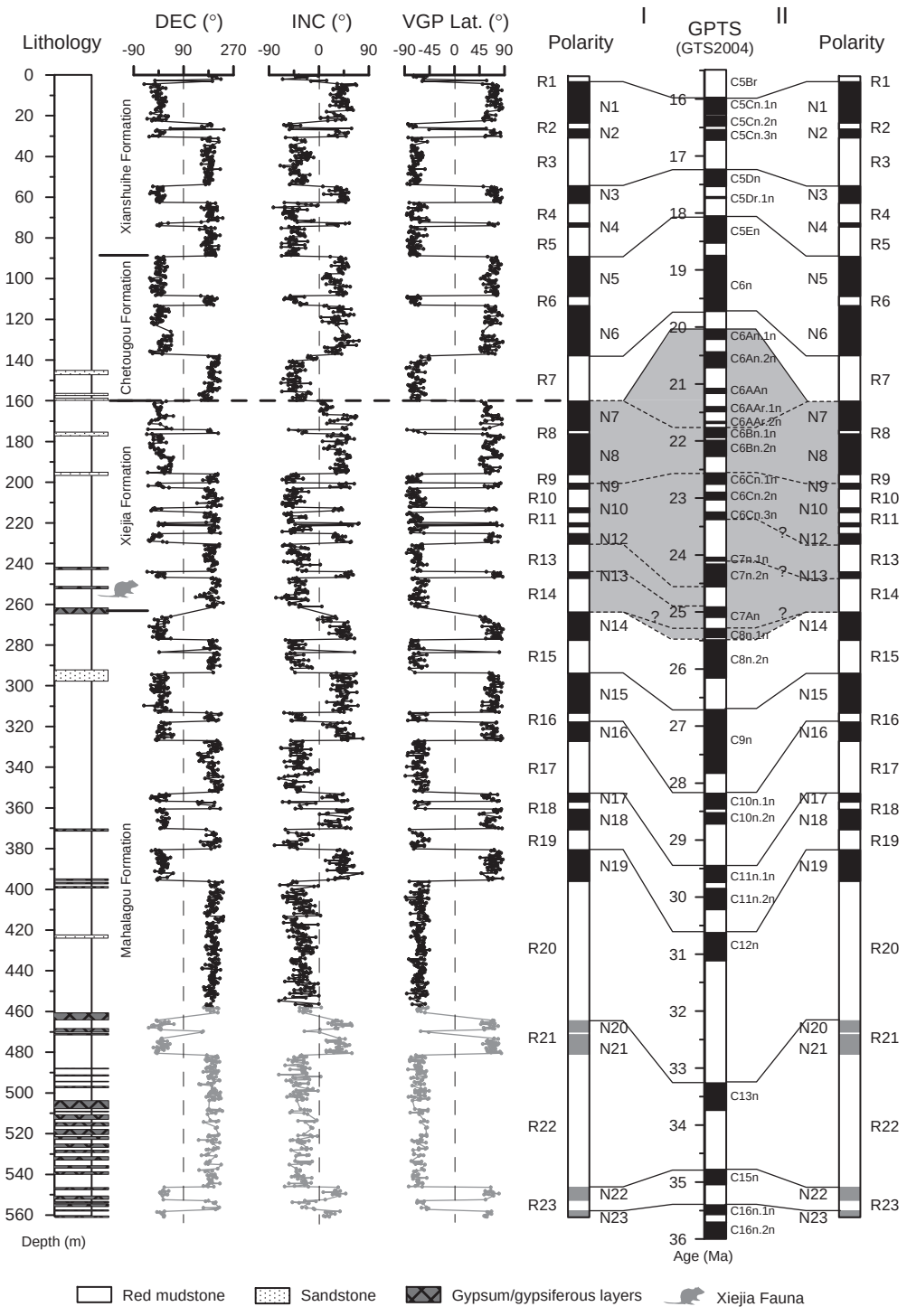

Fig. 5. Lithostratigraphy and magnetostratigraphy of the TS section, with the correlation to the GTS04 (Gradstein et al., 2004). Normal (reversed) polarity intervals labeled N1 to N23 (R1 to R23). The dashed line at the depth of ~160 m indicates the position of the unconformity. The gray dots and polarity below 457.5 m show the data from Xiao et al. (2010). The Xiejia Fauna found in the Xiejia section corresponds to the depth of ~252 m in the TS section, see the text for details.

(2006) from the Xiejia section ~3 km east of the TS section. Overall, our results can be well correlated to the upper 400 m of the Xiejia section of Dai et al. (2006) by stratigraphy and paleomagnetic polarity patterns. The paleomagnetic age of Xiejia Fauna correlated at ~252 m in the TS section in reversed polarity zone R14 between 25.5 and 24 Ma is consistent with Dai et al. (2006). However there are two important differences. The first is that our results show more short polarity zones than those in Dai et al. (2006), e.g., N9 and N16 are missing in their results; this is likely due to their larger sampling interval (1–2 m). Second, our results reveal a disconformity at ~160 m and yield correlations to the GPTS for N7-R13 that are different from the correlations in Dai et al. (2006). The magnetostratigraphic results of Wu et al. (2006), which yield a younger age for the Xiejia Fauna for the Xiejia section, are different from the measured polarity by Dai et al. (2006) and our study. A possible reason for this difference is that the studied interval of the section by Wu et al. (2006) only covers 250 m and includes the disconformity, making a miscorrelation to the GPTS more likely.

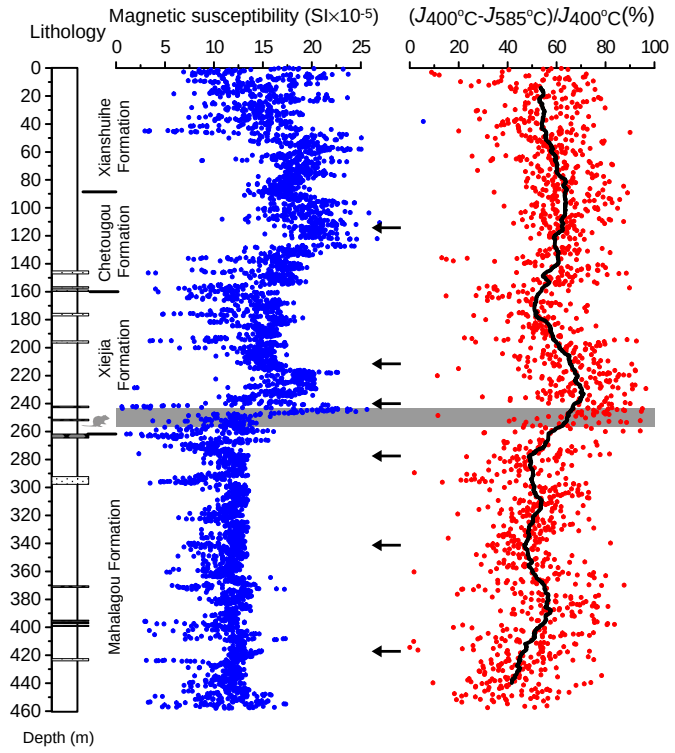

Fig. 6. The magnetic susceptibility and the ratio of $(J_{400\,°C}-J_{585\,°C})/J_{400\,°C}$ records of the Tashan section versus composite depth. The black arrows indicate the positions of samples used for thermomagnetic analysis (Fig. 4). Note that a noticeable increase in magnetic susceptibility and the ratios of $(J_{400\,°C}-J_{585\,°C})/J_{400\,°C}$ occurs at the depth of ~250 m as the gray bar shows. Symbology used in Fig. 6 is similar to Fig. 5.

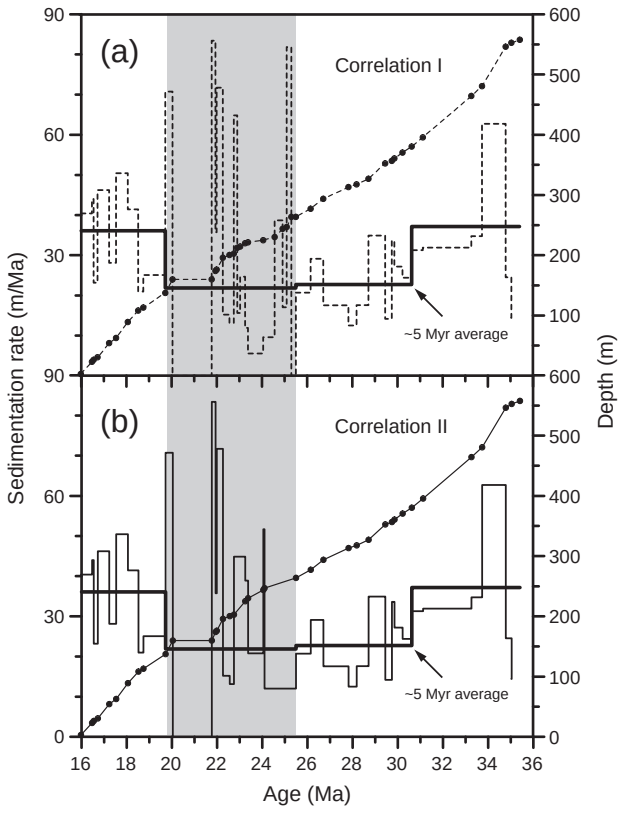

Fig. 7. Variations in sediment accumulation rate between ~35 and 16 Ma according to correlations I (a) and II (b). Note unstable accumulations during 25.3–19.7 Ma.

6. Discussion

6.1. NE Tibet tectonic implications

Based on the magnetostratigraphic age model obtained for the Xining Basin successions, sediment accumulation rates are low and nearly constant (average ~32 m/Myr) from ~33 Ma to ~16 Ma except for an unstable period during 25.3–19.7 Ma (Fig. 7). Averaged over longer time (~5 Myr), accumulation rates appear to be constant and low around 20 m/Myr from ~30 to ~20 Ma through the unstable interval but increase to ~30 m/Myr after that (Fig. 7). Remarkably, a recent thermochronological study showed that accelerated exhumation of the Laji Shan range, which defines the present southern edge of the Xining Basin, began at ~22 Ma (Lease et al., 2011). This strongly suggests that the exhumation of the Laji Shan is expressed by the coeval disturbance of sediment accumulation in the Xining Basin. In the same time interval (24–21 Ma), strata from the Hualong section in the Xunhua Basin a few kilometers south of the Laji Shan (Fig. 1), record increasing accumulation rates, changes in detrital zircon provenance and coarsening upwards lithologies interpreted as a response to increased flexural loading of the south-verging Laji Shan thrusting in a prograding foreland basin setting (Lease et al., in press). In contrast, in the TS section presently located ~25 km to the north from the Laji Shan range, the accelerated exhumation coincides with unstable accumulation rates but neither significant increase nor decrease when averaged over the disturbed interval (25.3–19.7 Ma, see Fig. 7). After this interval, however, long term accumulation rates significantly increase (Fig. 7). In terms of sedimentary facies, the disturbed 25–20 Ma interval is not distinctive compared to the rest of the investigated stratigraphy. It is dominated by massive lacustrine clays devoid of sedimentary structures and only two sand beds are present in the interval precluding significant provenance analysis. In comparison to the Xunhua section (Lease et al., in press), the lack of a typical prograding foreland basin response to exhumation may simply result from the Xining section being relatively far from the effects of flexural loading and sediment supply of the narrow Laji Shan range. This is in agreement with the relatively thin effective elastic thickness reported from this region (Braitenberg et al., 2003; DeCelles and Giles, 1996) and is substantiated by the Linxia sedimentary records (Maogou section, Fang et al., 2003) further away from the Laji Shan (Fig. 1) also showing lower accumulation rates, lower cumulative thicknesses and clay dominated facies as previously noted by Lease et al. (in press). Finally, the precise mechanism responsible for the observed unstable accumulation in association to Laji Shan exhumation remains to be determined. Speculatively, it may relate to forebulge migration inducing erosion followed by increased accumulation (DeCelles and Giles, 1996) or a delay in the north verging thrust initiation with respect to the south. We note, however, that in such arid underfilled systems, sediment accumulation is governed by sediment input rather than by subsidence (Carroll and Bohacs, 1999). Changes in supply, preservation/erosion and sedimentation are therefore more likely to explain the observed unstable accumulation rates although the precise link with the exhuming Laji Shan source and associated environmental changes remains elusive.

A link between the 25–20 Ma exhumation of the Laji Shan and the sedimentary input is substantiated by the coeval change in provenance indicated by the observed shift in sediment magnetic properties. The magnetic susceptibility and the remanence intensity ratio of $(J_{400\,°C}-J_{585\,°C})/J_{400\,°C}$ from the TS section have revealed permanent increase in magnetite at ~25 Ma (Fig. 8). Two general mechanisms have been typically proposed to explain increasing magnetite/hematite content: (1) pedogenic or diagenetic processes (perhaps climate controlled) that would favor magnetite over hematite concentrations; or (2) a change of provenance with a source containing more magnetite (e.g., Gilder et al., 2001; Sun et al., 2005). At this stage, option 1 is speculative as it requires extensive

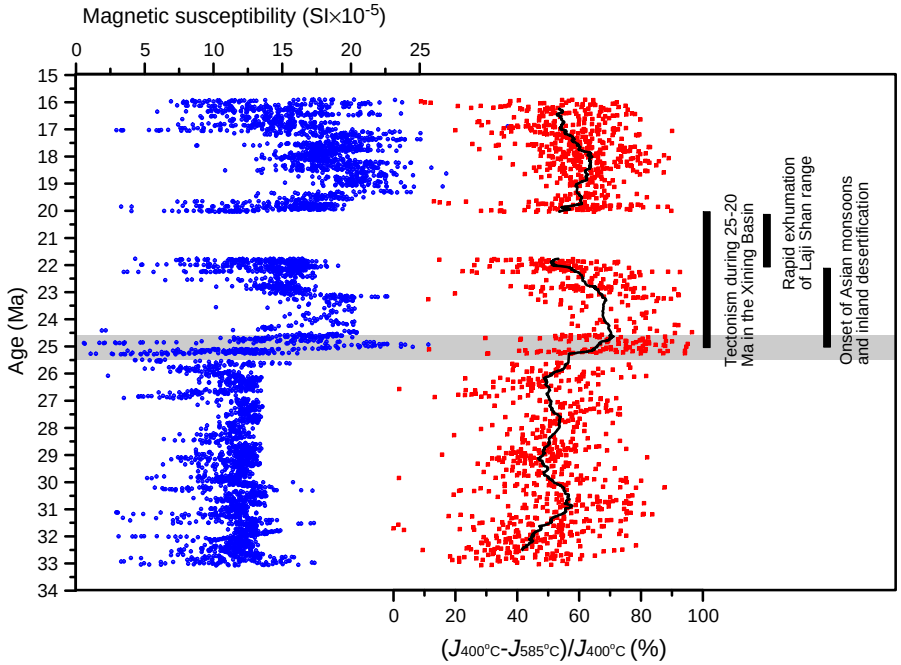

Fig. 8. The Tashan section magnetic susceptibility and the ratio of $(J_{400\,°C}-J_{585\,°C})/J_{400\,°C}$ records verses age in millions of years. The age model is based on correlation I (see text). The bold line superimposed on the ratio of $(J_{400\,°C}-J_{585\,°C})/J_{400\,°C}$ represents a 101-point running mean. The vertical bars indicate the timing of tectonism during 25–20 Ma in the Xining Basin (this study), rapid exhumation of Laji Shan range (Lease et al., 2011, in press), and onset of Asian monsoons and inland desertification (Guo et al., 2002, 2008; Sun and Wang, 2005), respectively.

rock magnetic data (e.g., Sun and Liu, 2000) to potentially establish the complex mechanisms responsible for magnetic mineral transformation during pedogenic or diagenetic processes. These processes would additionally have to be linked to eventual regional climate variations at this time. In comparison, a change in provenance (option 2) provides a more straightforward explanation. Before the Laji Shan exhumation, the most likely source of the Xining clastics is from the West Qinling Shan, which contains Triassic flysch and has been a source for sediments in the region since at least 50 Ma (Clark et al., 2010). We conclude that the best explanation for the increase in detrital magnetite is the ~25 Ma growth of Laji Shan, which is only tens of kilometers from the TS section and provides a recognized source of magnetite-rich plutonic and volcanic rocks (Lease et al., 2007, 2011; QBGMR, 1991). Moreover, mountain erosion is expected to produce a relatively larger influx of weakly weathered clastic materials due to shorter transport distances and quicker deposition. Both of these processes would decrease oxidation of incoming detrital magnetite into the basin, as has been reported in the Miocene red beds from northern Tibet (Gilder et al., 2001; Lu and Xiong, 2009; Sun et al., 2005).

The age of the uppermost strata found conformably above the TS section in the Xining Basin is estimated at ~14 Ma by extrapolating up the additional ~60 m of the Xianshuihe Formation using the 32 m/Myr accumulation rate. This age is close to the oldest fluvial-terrace loess which has been found in the Xining Basin (Lu et al., 2004), suggesting that the Xining Basin deposition was finally disrupted by incision and the formation of eolian deposits on these terraces. This age is also close to the reported ~13 Ma exhumation of the Jishi Shan associated with a regional tectonic reorganization and basin segmentation (Hough et al., 2011; Lease et al., 2011, in press; Wang et al., in press) which may be responsible for the final disruption and the incision of the Xining Basin.

6.2. Regional implications

Evidence for significant exhumation and deformation of the Himalayan–Tibetan Plateau is widespread during the 25–20 Ma period (e.g., Harrison et al., 1992; Zhang et al., 2010). Thermochronological results from nearby Qilian Shan indicate accelerated erosion ca. 20 Ma (e.g., George et al., 2001). The onset of exhumation and deformation is also reported at 25–20 Ma in the Tian Shan, Altyn Tagh, Western and Eastern Kunlun regions (e.g., Jolivet et al., 2001; Sobel et al., 2006). These results are consistent with the sedimentary record in adjacent basins (e.g., Ritts et al., 2004; Zhuang et al., 2011). In north-central Tibet, magnetostratigraphic investigation and field observation from the Tongtianhe section in the Hoh Xil Basin show that the Yaxicuo Group and Wudaoliang Group were separated by a pronounced angular unconformity, with an age about 23 Ma (Wang et al., 2008). The Quxu pluton exposed along the southern margin of the Lhasa terrance, near Lhasa city, was rapidly exhumed beginning at about 21 Ma (Harrison et al., 1992). Farther south, the oldest synkinematic micas within the Main Central Thrust have been dated at 24–21 Ma (Hodges et al., 1996; Yin et al., 1994), which is broadly in line with the timing of abrupt increase of the $^{87}Sr/^{86}Sr$ ratios in seawater that is attributed to the rapid exhumation of the Greater Himalayan metasedimentary rocks at ~20 Ma (Harris, 1995).

Increased surface elevations associated to this widespread evidence for deformation is supported by paleoaltimetry datasets from this time period (Quade et al., 2011). The Kailas Formation within the Indus-Yarlung suture zone records an abrupt change from rapidly deposited, northerly derived sediments indicative of humid, low-lying environments to southerly derived sediments deposited slowly in an arid, high elevation setting between ~24 and 22 Ma (DeCelles et al., 2011). Accurately dated ancient paleosol carbonates in the Nima Basin of central Tibet point to an arid climate and high paleoelevation (4.5–5 km, comparable to today's setting) by 26 Ma (DeCelles et al., 2007). The Nd isotope composition of sediments from the Hanoi Basin shows rapid changes during the latest Oligocene, implying large-scale drainage capture inferred to be associated with the surface uplift of Eastern Tibet (Clift et al., 2006). Thus, although we can not determine precise paleoelevations from our data, we conclude that the segmentation of the Xining Basin at 25–20 Ma is part of a larger, widespread pattern of tectonic deformation throughout the Himalaya and Tibetan Plateau, which may be

associated with significant surface uplift of the Tibetan Plateau that has been attributed to removal of mantle lithosphere from beneath Tibet (Molnar and Stock, 2009; Molnar et al., 1993).

Interestingly, this widespread surface uplift of the Tibetan Plateau is broadly coeval with a reported latest Oligocene to earliest Miocene reorganization of Asian climate (Fig. 8). The 25–20 Ma period is characterized by the strengthening of monsoon climate in Eastern Asia and the formation of central Asian deserts (Guo et al., 2002, 2008; Sun and Wang, 2005). Recent studies have shown that the timing of the initiation of the eolian deposits that were derived from Asian interior was around 25–20 Ma based on magnetostratigraphic dating (e.g., Guo et al., 2002; Hao and Guo, 2007; Qiang et al., 2011; Sun et al., 2010). This period is also marked by increasing erosion of the Himalayan and the start of foreland deposition of the Siwalik deposits that have been associated with the strengthening of the Indian monsoonal system (Clift et al., 2008). This is particularly interesting when considering that the Indian monsoon and East Asian monsoon appear to be dynamically different and forced by distinct boundary conditions (Molnar et al., 2010). Although the two monsoons may be intimately related, Boos and Kuang (2010) showed that the large-scale South Asian monsoon could be produced in a climate model with idealized Himalayan topography but without plateau while Molnar et al. (2010) argue the East Asian monsoon is primarily governed by the plateau forming an obstacle altering the jet stream. Thus, the onset of East Asian monsoon-like condition and aridity may have less to do with cumulative regional surface uplift of the Tibetan Plateau, per se, than closure of major downstream atmospheric and oceanic gateways due to the growth of specific and widely separated mountain ranges in the 25–20 Ma period. Climate models have also demonstrated that the aridification of central Asia may be related with the withdrawal of Paratethys in addition to increased orography (Guo et al., 2008; Ramstein et al., 1997; Zhang et al., 2007a, 2007b). However, the timing of the last major withdrawal of the Paratethys out of the Tarim Basin is older (37 Ma; see Bosboom et al., 2011), suggesting that the ~25–20 Ma transition of paleoenvironmental patterns in China is more likely related to Tibetan Plateau growth at this time rather than Paratethys retreat. Many recent works report ~45–40 Ma and ~15–10 Ma events (e.g., Molnar and Stock, 2009; Wang et al., 2008) beyond the context of the NE Tibetan plateau undergoing what appears to be short, discrete deformation events since ~50 Ma. The 25–20 Ma event is therefore probably not the only regionally important one although it appears to extend considerably from the Himalayas to the Tian Shan and NE Tibet and to be coeval with major Asian and Indian monsoonal changes.

Finally, despite the clear local contribution of the Laji Shan uplift to the shift in magnetic susceptibility observed in the TS section at ~25 Ma, we cannot discard the possibility of a more regional contribution since Asian eolian records typically appear to have magnetite from proximal as well as distal sources (e.g., Sun and Liu, 2000). A distal source may be associated with the coeval tectonism of Tibet at ~25–20 Ma and the major reorganization of East Asian climate. The grain size of the sediments in the TS section is similar to typical eolian material derived from central Asian deserts that has widely contributed sediments to the leeward sites in Western China (e.g., Garzione et al., 2005; Guo et al., 2002; Hao and Guo, 2007; Qiang et al., 2011; Sun et al., 2010), including the Xining Basin (Lu et al., 2004; Wang et al., 2006), and even the Pacific Ocean (Rea et al., 1985; Ziegler et al., 2007). Further evidence from provenance and grain size is required to test this hypothesis.

7. Conclusions

High-resolution magnetostratigraphic dating of the 460-m-thick Tashan section shows that it is earliest Oligocene (~33 Ma) to middle Miocene (~16 Ma) in age. A period of unstable sedimentation is observed from ~25 Ma to ~20 Ma, and we identify major depositional irregularities from ~25 to ~20 Ma, followed by increased accumulation. The timing is exactly coeval with the reported ~22 Ma accelerated exhumation of the nearby Laji Shan range, which is more generally linked to regional deformation of the northeastern margin of the Tibetan Plateau during this period. The recording of this tectonic pulse in our sedimentary record is confirmed by increased magnetite susceptibility at ~25 Ma, which we interpret as a change from a more regional source (possibly flysch in the Qinling Shan) to the more proximal volcanics in the Laji Shan that contain more magnetite. The change in provenance at ~25 Ma, about 3 Myr before the accelerated exhumation at ~22 Ma revealed by low-temperature thermochronometry, suggests that the sediments recorded the initial phases of mountain uplift preceding the main tectonic phase, or that erosion has removed the earliest record of exhumation in the Laji Shan. This may reflect a lag-time between rock-uplift and unroofing suggesting a bias to young exhumation ages with rock uplift dominating in such slowly-eroding, arid landscapes. Interestingly, both the sedimentary record and the thermochronological record suggest the Laji Shan grew rapidly up to ~20 Ma and has been eroded slowly since then.

Evidence for tectonism within the Xining Basin at 25–20 Ma can be associated with widespread deformation over the entire India–Asia collision zone at this time, from the Himalaya to the Tian Shan and to NE Tibet. Associated widespread surface uplift, rather than sea retreat occurring earlier in the middle Eocene, may be linked to the appearance of monsoon climate in Eastern Asia and the aridification of central Asian deserts reported at 25–20 Ma. Based on the suggested ~25–20 Ma link among the East Asian and Indian monsoons, increased aridity of Central Asia, and surface uplift of the Tibetan Plateau, we propose this was the time at which the plateau reached a threshold elevation or at which regional topography was organized in such a way as to change atmospheric circulation patterns.

Acknowledgments

We are grateful to Carmala N. Garzione and two anonymous reviewers for their thorough and constructive comments. This study is supported by the National Natural Science Foundation of China (projects 40730104) and the Foundation of Geological Survey of China (1212011121261). G. D.-N. and H. A. thank the Netherlands Organisation for Scientific Research (NWO-ALW) for funding. We thank Hongfu Yin, Baochun Huang, Chenglong Deng, and Junliang Ji for helpful suggestions. We are grateful to Jinfeng Liu, Bin Sun, Qiuzhen Yin, Meiyan Liang, Yanyan Yu, Xiaoyun Chen, Zhengquan Yao, Chenxi Xu, Tao Zhan and Chunlin Wu for field assistance.

References

Abels, H.A., Dupont-Nivet, G., Xiao, G.Q., Bosboom, R., Krijgsman, W., 2011. Step-wise change of Asian interior climate preceding the Eocene–Oligocene Transition (EOT). Palaeogeogr. Palaeoclimatol. Palaeoecol. 299, 399–412.

Boos, W.R., Kuang, Z.M., 2010. Dominant control of the South Asian monsoon by orographic insulation versus plateau heating. Nature 463, 218–222.

Bosboom, R.E., Dupont-Nivet, G., Houben, A.J.P., Brinkhuis, H., Villa, G., Mandic, O., Stoica, M., Zachariasse, W.J., Guo, Z., Li, C., 2011. Late Eocene sea retreat from the Tarim Basin (west China) and concomitant Asian paleoenvironmental change. Palaeogeogr. Palaeoclimatol. Palaeoecol. 299, 385–398.

Braitenberg, C., Wang, Y., Fang, J., Hsu, H.T., 2003. Spatial variations of flexure parameters over the Tibet–Quinghai Plateau. Earth Planet. Sci. Lett. 205, 211–224.

Carroll, A.R., Bohacs, K.M., 1999. Stratigraphic classification of ancient lakes: balancing tectonic and climatic controls. Geology 27, 99–102.

Clark, M.K., Farley, K.A., Zheng, D., Wang, Z., Duvall, A.R., 2010. Early Cenozoic faulting of the northern Tibetan Plateau margin from apatite (U–Th)/He ages. Earth Planet. Sci. Lett. 296, 78–88.

Clift, P.D., Blusztajn, J., Nguyen, A.D., 2006. Large-scale drainage capture and surface uplift in eastern Tibet–SW China before 24 Ma inferred from sediments of the Hanoi Basin, Vietnam. Geophys. Res. Lett. 33, L19403. doi:10.1029/2006GL027772.

Clift, P.D., Hodges, K.V., Heslop, D., Hannigan, R., Van Long, H., Calves, G., 2008. Correlation of Himalayan exhumation rates and Asian monsoon intensity. Nat. Geosci. 1, 875–880.

Dai, S., Fang, X.M., Dupont-Nivet, G., Song, C., Gao, J., Krijgsman, W., Langereis, C., Zhang, W., 2006. Magnetostratigraphy of Cenozoic sediments from the Xining Basin: tectonic implications for the northeastern Tibetan Plateau. J. Geophys. Res. 111, B11102. doi:10.1029/2005JB004187.
Dayem, K.E., Molnar, P., Clark, M.K., Houseman, G.A., 2009. Far-field lithospheric deformation in Tibet during continental collision. Tectonics 28. doi:10.1029/2008TC002344.
DeCelles, P.G., Giles, K.A., 1996. Foreland basin systems. Basin Res. 8, 105–123.
DeCelles, P.G., Quade, J., Kapp, P., Fan, M., Dettman, D.L., Ding, L., 2007. High and dry in central Tibet during the Late Oligocene. Earth Planet. Sci. Lett. 253, 389–401.
DeCelles, P.G., Kapp, P., Quade, J., Gehrels, G.E., 2011. Oligocene–Miocene Kailas basin, southwestern Tibet: record of postcollisional upper-plate extension in the Indus–Yarlung suture zone. Geol. Soc. Am. Bull. 123, 1337–1362.
Dettman, D.L., Fang, X.M., Garzione, C.N., Li, J.J., 2003. Uplift-driven climate change at 12 Ma: a long ^{18}O record from the NE margin of the Tibetan Plateau. Earth Planet. Sci. Lett. 214, 267–277.
Dunlop, D.J., Özdemir, Ö., 1997. Rock Magnetism: Fundamentals and Frontiers. Cambridge University Press, Cambridge, pp. 1–573.
Dupont-Nivet, G., Butler, R.F., Yin, A., Chen, X.H., 2003. Paleomagnetism indicates no Neogene vertical axis rotations of the northeastern Tibetan Plateau. J. Geophys. Res. 108, 2386. doi:10.1029/2003JB002399.
Dupont-Nivet, G., Horton, B.K., Zhou, J., Waanders, G.L., Butler, R.F., Wang, J., 2004. Paleogene clockwise tectonic rotation of the Xining–Lanzhou region, northeastern Tibetan Plateau. J. Geophys. Res. 109, B04401. doi:10.1029/2003JB002620.
Dupont-Nivet, G., Krijgsman, W., Langereis, C.G., Abels, H.A., Dai, S., Fang, X.M., 2007. Tibetan plateau aridification linked to global cooling at the Eocene–Oligocene transition. Nature 445, 635–638.
Dupont-Nivet, G., Hoorn, C., Konert, M., 2008a. Tibetan uplift prior to the Eocene–Oligocene climate transition: evidence from pollen analysis of the Xining Basin. Geology 36, 987–990.
Dupont-Nivet, G., Dai, S., Fang, X.M., Krijgsman, W., Erens, V., Reitsma, M., Langereis, C., 2008b. Timing and distribution of tectonic rotations in the northeastern Tibetan Plateau. In: Burchfiel, B.C., Wang, E. (Eds.), Investigations into the Tectonics of the Tibetan Plateau: Geol. Soc. Spec. Publ., 444, pp. 73–87.
Fang, X.M., Garzione, C., Van der Voo, R., Li, J.J., Fan, M.J., 2003. Flexural subsidence by 29 Ma on the NE edge of Tibet from the magnetostratigraphy of Linxia Basin, China. Earth Planet. Sci. Lett. 210, 545–560.
Fang, X.M., Yan, M.D., Van der Voo, R., Rea, D.K., Song, C.H., Parés, J.M., Gao, J.P., Nie, J.S., Dai, S., 2005. Late Cenozoic deformation and uplift of the NE Tibetan Plateau: evidence from high-resolution magnetostratigraphy of the Guide Basin, Qinghai Province, China. Geol. Soc. Am. Bull. 117, 1208–1225.
Garzione, C.N., Ikari, M.J., Basu, A.R., 2005. Source of Oligocene to Pliocene sedimentary rocks in the Linxia basin in northeastern Tibet from Nd isotopes: implications for tectonic forcing of climate. Geol. Soc. Am. Bull. 117, 1156–1166.
Gautam, P., Fujiwara, Y., 2000. Magnetic polarity stratigraphy of Siwalik Group sediments of Karnali River section in western Nepal. Geophys. J. Int. 142, 812–824.
George, A.D., Marshallsea, S.J., Wyrwoll, K.-H., Jie, C., Chou, L.Y., 2001. Miocene cooling in the northern Qilian Shan, northeastern margin of the Tibetan Plateau, revealed by apatite fission-track and vitrinite-reflectance analysis. Geology 29, 939–942.
Gilder, S., Chen, Y., Sen, S., 2001. Oligo-Miocene magnetostratigraphy and rock magnetism of the Xishuigou section, Subei (Gansu Province, western China) and implications for shallow inclinations in central Asia. J. Geophys. Res. 106, 30505–30521.
Gradstein, F.M., Ogg, J.G., Smith, A.G., 2004. A Geologic Time Scale 2004. Cambridge University Press, Cambridge, pp. 1–589.
Guo, Z.T., Ruddiman, W.F., Hao, Q.Z., Wu, H.B., Qiao, Y.S., Zhu, R.X., Peng, S.Z., Wei, J.J., Yuan, B.Y., Liu, T.S., 2002. Onset of Asian desertification by 22 Myr ago inferred from loess deposits in China. Nature 416, 159–163.
Guo, Z.T., Sun, B., Zhang, Z.S., Peng, S.Z., Xiao, G.Q., Ge, J.Y., Hao, Q.Z., Qiao, Y.S., Liang, M.Y., Liu, J.F., Yin, Q.Z., Wei, J.J., 2008. A major reorganization of Asian climate by the early Miocene. Clim. Past 4, 153–174.
Hao, Q.Z., Guo, Z.T., 2007. Magnetostratigraphy of an early-middle Miocene loess-soil sequence in the western Loess Plateau of China. Geophys. Res. Lett. 34, L18305. doi:10.1029/2007GL031162.
Hao, Y.C., Ruan, P.H., Zhou, X.G., Song, Q.S., Yang, G.D., Cheng, S.W., Wei, Z.X., 1983. Middle Jurassic–Tertiary deposits and ostracod–charophyte fossil assemblages of Xining and Minhe Basins. Earth Sci. J. China Univ. Geosci. 8, 1–221 (in Chinese with English abstract).
Harris, N., 1995. Significance of weathering Himalayan metasedimentary rocks and leucogranites for the Sr isotope evolution of sea water during early Miocene. Geology 23, 795–798.
Harrison, T.M., Copeland, P., Kidd, W.S.F., Yin, A., 1992. Raising Tibet. Science 255, 1663–1670.
Hodges, K.V., Parrish, R.R., Searle, M.P., 1996. Tectonic evolution of the central Annapurna Range, Nepalese Himalayas. Tectonics 15, 1264–1291.
Horton, B.K., Dupont-Nivet, G., Zhou, J., Waanders, G.L., Butler, R.F., Wang, J., 2004. Mesozoic–Cenozoic evolution of the Xining–Minhe and Dangchang basins, northeastern Tibetan Plateau: magnetostratigraphic and biostratigraphic results. J. Geophys. Res. 109, B04402. doi:10.1029/2003JB002913.
Hough, B.G., Garzione, C.N., Wang, Z.C., Lease, R.O., Burbank, D.W., Yuan, D.Y., 2011. Stable isotope evidence for topographic growth and basin segmentation: implications for the evolution of the NE Tibetan Plateau. Geol. Soc. Am. Bull. 123, 168–185.
Ji, J.L., Zhang, K.X., Tai, Q., Kou, X.H., Chen, F.N., Xu, Y.D., Lu, J.F., Lin, Q.X., 2010. Magnetostratigraphy of the Neogene strata in the Xunhua Basin, Qinghai Province. Earth Sci. J. China Univ. Geosci. 35, 803–810 (in Chinese with English abstract).
Jolivet, M., Brunel, M., Seward, D., Xu, Z., Yang, J., Roger, F., Tapponnier, P., Malavieille, J., Arnaud, N., Wu, C., 2001. Mesozoic and Cenozoic tectonics of the northern edge of the Tibetan plateau: fission-track constraints. Tectonophysics 343, 111–134.
Kent, D.V., Muttoni, G., 2008. Equatorial convergence of India and early Cenozoic climate trends. Proc. Natl. Acad. Sci. 105, 16065–16070.
Kirschvink, J.L., 1980. The least-squares line and plane and the analysis of palaeomagnetic data. Geophys. J. R. Astron. Soc. 62, 699–718.
Lease, R.O., Burbank, D.W., Gehrels, G.E., Wang, Z.C., Yuan, D.Y., 2007. Signatures of mountain building: detrital zircon U/Pb ages from northeastern Tibet. Geology 35, 239–242.
Lease, R.O., Burbank, D.W., Clark, M.K., Farley, K.A., Zheng, D., Zhang, H., 2011. Middle Miocene reorganization of deformation along the northeastern Tibetan Plateau. Geology 39, 359–362.
Lease, R O, Burbank, D W, Hough, B, Wang, Z C, Yuan, D Y. in press. Pulsed Miocene range growth in northeastern Tibet: insights from Xunhua basin magnetostratigraphy and provenance. Geol. Soc. Am. Bull.
Li, C.K., Qiu, Z.D., 1980. Early Miocene mammalian fossils of Xining Basin, Qinghai. Vertebrat. Palasiatic. 18, 198–214 (in Chinese with English abstract).
Li, C.K., Qiu, Z.D., Wang, S.J., 1981. Discussion on Miocene stratigraphy and mammals from Xining Basin, Qinghai. Vertebrat. Palasiatic. 19, 313–320 (in Chinese with English abstract).
Li, J.J., Fang, X.M., Van der Voo, R., Zhu, J.J., Niocaill, C.M., Cao, J.X., Zhong, W., Chen, H.L., Wang, J.L., MingWang, J., Zhang, Y.C., 1997. Late Cenozoic magnetostratigraphy (11–0 Ma) of the Dongshanding and Wangjiashan sections in the Longzhong Basin, western China. Geol. Mijnb. 76, 121–134.
Liu, M.R., 1992. Stratigraphic sequence and fossil assemblage of Neogene System in Xining–Minhe Basin. Qinghai Geol. 4, 1–18 (in Chinese with English abstract).
Lu, H.J., Xiong, S.F., 2009. Magnetostratigraphy of the Dahonggou section, northern Qaidam Basin and its bearing on Cenozoic tectonic evolution of the Qilian Shan and Altyn Tagh Fault. Earth Planet. Sci. Lett. 288, 539–550.
Lu, H.Y., Wang, X.Y., An, Z.S., Miao, X.D., Zhu, R.X., Ma, H.Z., Li, Z., Tan, H.B., Wang, X.Y., 2004. Geomorphologic evidence of phased uplift of the northeastern Qinghai–Tibet Plateau since 14 million years ago. Sci. China, Ser. D 47, 822–833.
Molnar, P., Stock, J.M., 2009. Slowing of India's convergence with Eurasia since 20 Ma and its implications for Tibetan mantle dynamics. Tectonics 28, TC3001. doi:10.1029/2008TC002271.
Molnar, P., England, P., Martinod, J., 1993. Mantle dynamics, the uplift of the Tibetan Plateau, and the Indian monsoon. Rev. Geophys. 31, 357–396.
Molnar, P., Boos, W.R., Battisti, D.S., 2010. Orographic controls on climate and paleoclimate of Asia: thermal and mechanical roles for the Tibetan Plateau. Annu. Rev. Earth Planet. Sci. 38, 77–102.
Pares, J.M., Van der Voo, R., Downs, W.R., Yan, M.D., Fang, X.M., 2003. Northeastward growth and uplift of the Tibetan Plateau: magnetostratigraphic insights from the Guide Basin. J. Geophys. Res. 108 (B1), 2017. doi:10.1029/2001JB001349.
QBGMR (Qinghai Bureau of Geology and Mineral Resources), 1991. Regional Geology of the Qinghai Province. Geological Publishing House, Beijing, pp. 1–662 (In Chinese).
QBGMR (Qinghai Bureau of Geology and Mineral Resources), 1985. Geologic maps of the Duoba, Gaodian, Tianjiazai, and Xining regions (4 sheets), with regional geologic report (1:50,000 scale), Geological Publishing House, Beijing (In Chinese).
Qiang, X., An, Z., Song, Y., Chang, H., Sun, Y., Liu, W., Ao, H., Dong, J., Fu, C., Wu, F., Lu, F., Cai, Y., Zhou, W., Cao, J., Xu, X., Ai, L., 2011. New eolian red clay sequence on the western Chinese Loess Plateau linked to onset of Asian desertification about 25 Ma ago. Sci. China, Ser. D. 54, 136–144.
Qiu, Z.X., Qiu, Z.D., 1995. Chronological sequence and subdivision of Chinese Neogene mammalian faunas. Palaeogeogr. Palaeoclimatol. Palaeoecol. 116, 41–70.
Quade, J., Breecker, D.O., Daeron, M., Eiler, J., 2011. The paleoaltimetry of Tibet: an isotopic perspective. Am. J. Sci. 311, 77–115.
Ramstein, G., Fluteau, F., Besse, J., Joussaume, S., 1997. Effect of orogeny, plate motion and land-sea distribution on Eurasian climate change over the past 30 million years. Nature 386, 788–795.
Raymo, M.E., Ruddiman, W.F., 1992. Tectonic forcing of late Cenozoic climate. Nature 359, 117–122.
Rea, D.K., Leinen, M., Janecek, T.R., 1985. Geologic approach to the long-term history of atmospheric circulation. Science 227, 721–725.
Ritts, B.D., Yue, Y.J., Graham, S.A., 2004. Oligocene–Miocene tectonics and sedimentation along the Altyn Tagh Fault, Northern Tibetan Plateau: analysis of the Xorkol, Subei, and Aksay Basins. J. Geol. 112, 207–229.
Royden, L.H., Burchfiel, B.C., van der Hilst, R.D., 2008. The geological evolution of the Tibetan Plateau. Science 321, 1054–1058.
Sobel, E., Chen, J., Heermance, R., 2006. Late Oligocene–Early Miocene initiation of shortening in the Southwestern Chinese Tian Shan: implications for Neogene shortening rate variations. Earth Planet. Sci. Lett. 247, 70–81.
Sun, J.M., Liu, T.S., 2000. Multiple origins and interpretations of the magnetic susceptibility signal in Chinese wind-blown sediments. Earth Planet. Sci. Lett. 180, 287–296.
Sun, X.J., Wang, P.X., 2005. How old is the Asian monsoon system?—Palaeobotanical records from China. Palaeogeogr. Palaeoclimatol. Palaeoecol. 222, 181–222.
Sun, J.M., Zhu, R.X., An, Z.S., 2005. Tectonic uplift in the northern Tibetan Plateau since 13.7 Ma ago inferred from molasse deposits along the Altyn Tagh Fault. Earth Planet. Sci. Lett. 235, 641–653.
Sun, J.M., Ye, J., Wu, W.Y., Ni, X.J., Bi, S.D., Zhang, Z.Q., Liu, W.M., Meng, J., 2010. Late Oligocene–Miocene mid-latitude aridification and wind patterns in the Asian interior. Geology 38, 515–518.
Tapponnier, P., Xu, Z.Q., Roger, F., Meyer, B., Arnaud, N., Wittlinger, G., Yang, J.S., 2001. Oblique stepwise rise and growth of the Tibet Plateau. Science 294, 1671–1677.
Tauxe, L., 1998. Paleomagnetic Principles and Practice. Kluwer Academic Publishers, Dordrecht, pp. 1–299.
Wang, Y., Deng, T., 2005. A 25 m.y. isotopic record of paleodiet and environmental change from fossil mammals and paleosols from the NE margin of the Tibetan Plateau. Earth Planet. Sci. Lett. 236, 322–338.

Wang, D.N., Sun, X.Y., Zhao, Y.N., 1990. Late Cretaceous to Tertiary palynofloras in Xinjiang and Qinghai, China. Rev. Palaeobot. Palynol. 65, 95–104.
Wang, X.Y., Lu, H.Y., Ji, J.F., Wang, X.Y., Zhao, J.B., Huang, B.C., Li, Z., 2006. Origin of the Red Earth sequence on the northeastern Tibetan Plateau and its implications for regional aridity since the Middle Miocene. Sci. China, Ser. D 49, 505–517.
Wang, C.S., Zhao, X.X., Liu, Z.F., Lippert, P.C., Graham, S.A., Coe, R.S., Yi, H.S., Zhu, L.D., Liu, S., Li, Y.L., 2008. Constraints on the early uplift history of the Tibetan Plateau. Proc. Natl. Acad. Sci. 105, 4987–4992.
Wang, Z, Zhang, P Z, Garzione, C N, Lease, R O, Zhang, G L, Zheng, D, Hough, B, Yuan, D Y, Chuan You Li, Liu, J H, Wu, Q L. in press. Magnetostratigraphy and depositional history of the Miocene Wushan basin on the NE Tibetan plateau, China: implications for middle Miocene tectonics of the West Qinling fault zone. J. Asian Earth Sci.
Wu, L.C., Yue, L.P., Wang, J.Q., Heller, F., Deng, T., 2006. Magnetostratigraphy of stratotype section of the Neogene Xiejian Stage. J. Stratigr. 30, 50–53 (in Chinese with English abstract).
Xiao, G.Q., Abels, H.A., Yao, Z.Q., Dupont-Nivet, G., Hilgen, F.J., 2010. Asian aridification linked to the first step of the Eocene–Oligocene climate Transition (EOT) in obliquity-dominated terrestrial records (Xining Basin, China). Clim. Past 6, 501–513.
Yan, M., Van der Voo, R., Fang, X., Parés, J.M., Rea, D.K., 2006. Paleomagnetic evidence for a mid-Miocene clockwise rotation of about 25° of the Guide Basin area in NE Tibet. Earth Planet. Sci. Lett. 241, 234–247.
Yin, A., Harrison, T.M., Ryerson, F.J., Wenji, C., Kidd, W.S.F., Copeland, P., 1994. Tertiary structural evolution of the Gangdese thrust system, southeastern Tibet. J. Geophys. Res. 99, 18175–18201.
Yue, L.P., Heller, F., Qiu, Z.X., Zhang, L., Xie, G.P., Qiu, Z.D., Zhang, Y.X., 2001. Magnetostratigraphy and paleoenvironmental record of Tertiary deposits of Lanzhou Basin. Chin. Sci. Bull. 46, 770–773.
Zhang, Z.S., Wang, H.J., Guo, Z.T., Jiang, D.B., 2007a. Impacts of tectonic changes on the reorganization of the Cenozoic paleoclimatic patterns in China. Earth Planet. Sci. Lett. 257, 622–634.
Zhang, Z.S., Wang, H.J., Guo, Z.T., Jiang, D.B., 2007b. What triggers the transition of palaeoenvironmental patterns in China, the Tibetan Plateau uplift or the Paratethys Sea retreat? Palaeogeogr. Palaeoclimatol. Palaeoecol. 245, 317–331.
Zhang, K.X., Wang, G.C., Ji, J.L., Luo, M.S., Kou, X.H., Wang, Y.M., Xu, Y.D., Chen, F.N., Chen, R.M., Song, B.W., Zhang, J.Y., Liang, Y.P., 2010. Paleogene–Neogene stratigraphic realm and sedimentary sequence of the Qinghai–Tibet Plateau and their response to uplift of the plateau. Sci. China, Ser. D 53, 1271–1294.
Zheng, D.W., Zhang, P.Z., Wan, J.L., Li, C.Y., Cao, J.X., 2003. Late Cenozoic deformation subsequence in northeastern margin of Tibet — Detrital AFT records from Linxia Basin. Sci. China, Ser. D 46, 266–275.
Zheng, D.W., Zhang, P.Z., Wan, J.L., Yuan, D.Y., Li, C.Y., Yin, G.M., Zhang, G.L., Wang, Z.C., Min, W., Chen, J., 2006. Rapid exhumation at 8 Ma on the Liupan Shan thrust fault from apatite fission-track thermochronology: implications for growth of the northeastern Tibetan Plateau margin. Earth Planet. Sci. Lett. 248, 198–208.
Zhuang, G., Hourigan, J.K., Ritts, B.D., Kent-Corson, M.L., 2011. Cenozoic multiple-phase tectonic evolution of the northern Tibetan Plateau: constraints from sedimentary records from Qaidam basin, Hexi Corridor, and Subei basin, northwest China. Am. J. Sci. 311, 116–152.
Ziegler, C.L., Murray, R.W., Hovan, S.A., Rea, D.K., 2007. Resolving eolian, volcanogenic, and authigenic components in pelagic sediment from the Pacific Ocean. Earth Planet. Sci. Lett. 254, 416–432.